Montmorillonite Clay Nanocomposites of Sulfonic Acid Doped Thermoreversible Polyaniline Gel: Physical and Mechanical Properties

Ashesh Garai, Biplab K. Kuila, and Arun K. Nandi*

Polymer Science Unit, Indian Association for the Cultivation of Science, Jadavpur, Kolkata 700 032, India

Received March 22, 2006; Revised Manuscript Received June 5, 2006

ABSTRACT: Polyaniline (PANI)−dinonylnaphthalene disulfonic acid (DNNDSA) form a thermoreversible gel when prepared from formic acid medium. Mixing of organically modified montmorillonite (om-MMT) clay during PANI−DNNDSA gel preparation produces the PANI−DNNDSA gel nanocomposites (GNCs). WAXS and TEM pictures indicate GNC-1 (number indicates percentage (w/w) of om-clay in the nanocomposite) has an exfoliated structure, whereas GNC-3 and GNC-5 have an intercalated structure. FTIR spectra indicate an interaction between om-clay and PANI−DNNDSA shifting the Q=N^+H−B or B−N^+H−B (Q = quinonoid and B = benzonoid unit of PANI) vibration of quinonoid structure to lower energy. The exfoliated GNC-1 has higher thermal stability than that of the intercalated GNC-3 and GNC-5 samples. The storage modulus (G') has increased dramatically on addition of clay to the gel and its relative increase is larger with increase in temperature until the gel melts. The highest increase (445%) of G' is observed for GNC-1 at 60 °C. The π band−polaron band position remains unaffected by the addition of clay in the gel and so also the dc conductivity. PANI−DNNDSA gel shows emission at 353 nm when excited with a radiation of 262 nm. But in the GNCs, fluorescence quenching occurs and it is maximum for the exfoliated GNC-1 sample. These GNCs of PANI are easily processable due to its thermoreversible nature.

Introduction

Polymer−clay nanocomposites (PNCs) have received considerable research interest because of the dramatic improvement in physical and mechanical properties.[1−6] Apart from the PNCs of commodity plastics, the PNCs of specialty polymers, e.g., conducting polymers, are now widely studied not only to increase the mechanical and physical properties but also to improve the conducting and optoelectronic properties of these materials.[7−21] Polyaniline (PANI) is an important conducting polymer because of its high conductivity,[22] unique redox property,[23] and easier method of synthesis,[24] but it is very difficult to process because of its high aromatic nature, strong interchain hydrogen bonding, and high charge delocalization.[25,26] Now, long-chain sulfonic acids and phosphoric acids are used as both doping agents and processing aids to PANI installed by various ways, e.g., dispersion polymerization,[27,28] emulsion polymerization,[29] mechanical mixing,[30] and solvent cast mixing.[31] But a slightly different approach of doping with sulfonic acid using the swelled PANI lattice in a formic acid medium produces thermoreversible gels when the long-chain sulfonic acids are used in larger concentrations (>50% w/w).[32−37] In this article, we explore the effect of montmorillonite (organically modified) clay on the physical, mechanical, and conducting properties of these types of gels.

Montmorillonite (MMT) is a clay mineral and consists of two fused silicate tetrahedral sheets sandwiching an edge-shared octahedral sheet of either magnesium or aluminum hydroxide[1]. The staked silicate sheets (thickness ∼1 nm, length ∼218 nm) have a platelet-like structure with a high aspect ratio (220).[38] In the interlayer, there exist Na^+ and Ca^{2+}, which can be replaced by the alkylammonium and phosphonium ions transforming the clay into an organophilic nature.[1,39] The organic modifier may enhance the interaction between the clay and polymer and it may favor the intercalation of a polymer chain by dictating the gallery spacing. The PANI−long-chain sulfonic acid systems prepared from formic acid medium produce thermoreversible gels where the sulfonic acid groups are anchored with the aminic or iminic nitrogen atoms of PANI.[32−37] The comb-shaped polymers have pendent hydrocarbon tails, which have a possibility of interaction with the alkyl tails of organically modified MMT (om-MMT) clay as in the poly(3-hexyl thiophene) (P3HT)−MMT nanocomposites.[17,18] As a result, dispersion of the clay tactoids in the blend is expected and this would dramatically improve the mechanical and physical properties of PANI−surfactant gel because the clay tactoids have the dimensions in the nanorange (thickness ∼1 nm and length ∼218 nm). This high aspect ratio (∼220) of the clay tactoids may enhance the physical and mechanical properties of the PANI−surfactant gels. This study, therefore, adds the processing ability of PANI with the improvement of its physical and mechanical properties to render its use in different technological applications. The effect of nanoclay on the mechanical properties of the gels is not yet reported, so this study is important to understand how the clay particles affect the mechanical properties of PANI−DNNDSA gel.

In our previous reports of P3HT/clay nanocomposites, it was observed that the conductivity of the undoped P3HT remains almost invariant with that of pure P3HT both for solvent-cast and melt-cooled samples. Here, we also expect similar behavior in conductivity, i.e., it may be possible to enhance the mechanical and physical properties of GNCs without any scarification of conductivity. The *p*-type polymers, e.g., poly(*p*-phenylenes), polyfluorene, and polythiophenes, usually exhibit photoluminescence with the holes as major carrier.[8] Lee at al. obtained enhancement of photoluminescence by making PNCs of poly(2-methoxy-5,2′-ethylhexyloxy-1,4-phenylene vi-

* Corresponding author. E-mail: psuakn@mahendra.iacs.res.in.

10.1021/ma060636w CCC: $33.50
Published on Web 07/06/2006

nylene) (MEH-PPV).[8] In P3HT, we observed photoluminescence quenching in the solvent-cast PNCs, but in the melt-cooled PNCs, the quantum yield of the photoluminescence process has increased.[17,18] Usually, confinement of charge carriers within the clay tactoids increases the photoluminescence efficiency,[8] but the presence of a fibrillar network structure in the solvent-cast PNCs promotes the energy transfer of a charge carrier through the network, causing photoluminescence quenching.[18] In this article, we shall delineate these important properties of sulfonic acid doped PANI and its nanocomposites. Thus, a complete study of polymer−clay nanocomposite of sulfonic acid doped polyaniline gel is presented here.

Experimental Section

a. Sample. Polyaniline was prepared in the laboratory by polymerizing distilled aniline in HCl medium with ammonium persulfate as an initiator.[24] The polyaniline salt was converted to emeraldine base (EB) form by digesting with NH_4OH solution. The PANI (EB) was characterized by viscosity measurement in H_2SO_4 (97%). The intrinsic viscosity [η] was measured to be 0.972 g/dl at 25 °C. The molecular weight of PANI was found to be 15 500, calculated by the approximation of taking k and α values of poly(*p*-phenylene terephthalamide) [$k = 1.95 \times 10^{-6}$ and $\alpha = 1.36$] in H_2SO_4 medium.[40,41]

Dopant. Dinonylnaphthalene disulfonic acid (DNNDSA) was a gift sample from King Industries (Norwalk, CT) with a trade name of Nacure 155. The DNNDSA was supplied as 55% concentrate in isobutanol.

Solvent. The formic acid (synthesis grade, E. Merck, India) and H_2SO_4 (97%) (E. Merck, India) were used as received. The *N*,*N*-dimethyl fomamide (DMF) (G. R. Merck, India) used for spectophotometric measurements was dried over CaH_2 and was then fractionally distilled. The middle portion was used in the work.

b. Preparation of the Gel Nanocomposite (GNC). PANI (EB) and DNNDSA in the weight ratio (15:85) (the weight of DNNDSA was counted from its 55% (w/w) concentration in isobutanol in each case.) were mixed in formic acid medium (total concentration 2.5% (w/w)) in a round-bottomed flask. The weight of om-clay was chosen such that the total clay concentrations in the system were 1%, 3%, and 5%, with respect to the weight of PANI−DNNDSA (w/w). They were stirred at 65 °C in an oil bath by magnetic stirrer for 24 h. The mixtures were then dried on flat dishes at 60 °C in a mild flow of air. Finally, they were dried at 60 °C in a vacuum for 1 week. The FTIR studies of the dried sample clearly indicate the absence of the 3114 cm^{-1} peak, indicating the absence of formic acid in the dried sample. Also, there were no peak at 3337 cm^{-1} in the FTIR spectra, characterizing the removal of isobutanol during the drying[34] (Figure 1, Supporting Information). For the preparation of GNCs, the MMT clay was organically modified. The MMT clay (PGV-PV-178-00), a product of Nanocor, Arlington Height, IL, was organically modified by dispersing the clay in water and adding cetyl trimethylammonium bromide (CTAB) in a weight ratio of 2:1. It was then stirred for 12 h, and the modified clay was collected by centrifugation (11 000 rpm). Excess CTAB was removed by repeated centrifugation with water and monitoring the removal of bromide ion by the $AgNO_3$ test. It was then dried in a vacuum for 3 days, and the exchange capacity of the clay was measured to be 101.4 mequiv/100 g by thermogravimetric analysis.[17,42]

The gel nanocomposites (GNCs) were prepared by dispersing the required amount of om-clay in formic acid and mixing it with the formic acid solution of PANI (EB) and DNNDSA. The mixture was stirred for 24 h in a thermostatic oil bath at 65 °C by magnetic stirrer as was done earlier. The mixture was then dried at 60 °C in a flat dish on a pool of air. Finally they were dried at 60 °C in a vacuum for 7 days. The absence of formic acid and isobutanol was tested from FTIR studies of dried samples (Figure 1, Supporting Information). The absence of the peaks at 3114 and 3337 cm^{-1} correspond to the absence of formic acid and isobutanol, respectively.[34,43] The clay composites are designated as GNC-1, GNC-3, and GNC-5, where the number indicates the weight percentage of clay in the composites.

c. Morphology. The morphology of the samples was studied by both TEM and FE-SEM instruments. For TEM study, a thin section (∼70 nm) of the above nanocomposite was made by encapsulating it in an epoxy matrix and cutting at 25 °C through an ultramicrotome (Ultracut R, Leica) equipped with a glass knife. It was then placed on a carbon-coated copper grid and was observed through a high-resolution transmission electron microscope (JEOL, 2010 EX). It was operated at an accelerated voltage of 200 kV without staining. A CCD camera was used to take the picture.

The morphology of the dried gels was recorded in a field emission scanning electron microscope (FE-SEM) apparatus (JEOL, JSM-6700F). The samples were platinum coated on the surface and were observed at a voltage of 4 kV.

d. Structure. The structure of the gel and its nanocomposites was determined using a WAXS instrument (Seifert X-ray diffractometer, model C-3000) in reflecting mode with a parallel beam optics attachment. Nickel-filtered Cu Kα radiation ($\lambda = 0.154$ nm) operating at a 35 kV voltage and a 30 mA current was used. The samples were scanned from $2\theta = 1.5-37°$ at the step-scan mode (step size 0.03°, preset time 2 s), and the diffraction pattern was recorded using a scintillation counter detector.

e. Spectral characterization. The UV−vis spectra of the GNCs were made in dimethyl formamide (DMF) solution from 200 to1100 nm wavelength in a UV−vis spectrophotometer (model 8453, Hewlett-Packard). The solvent spectrum was subtracted from the solution (0.15% w/v) spectra, and both were taken in a quartz cell with a 1 mm path length. The photoluminescence experiments of gels were done in a Perkin-Elmer instrument (LS55 luminescence spectrometer). The sample of uniform thickness was made by equal spreading of 0.2 mL formic acid solution (2.5% w/w) over an equal area of a glass slide and then drying at 60 °C and finally in a vacuum. The photoexcitation was made at an excitation wavelength of 226 nm at a 45° angle of the film plane. The emission was detected at a right angle to the excitation beam direction.

The FTIR spectra of the samples were performed from the KBr pellets of the samples in a Nicolet FTIR instrument (Magna-IR-750 spectrometer (series-11)).

f. Thermal Measurement. The differential scanning calorimetry (DSC) experiments were performed in a Perkin-Elmer DSC-7 fitted with intracooler-1 and working under N_2 atmosphere. The samples were taken in large volume capsules (LVC) and heated from −30 to 160 °C at the heating rate of 10 °C/min. Cooling runs were also made after waiting for 10 min at 160 °C and then cooled at the rate of 5 °C/min to −30 °C. It was then again heated at the rate of 10 °C/min to 160 °C. The melting point and enthalpy of fusion values were measured by a computer attached to the instrument using PC-series DSC-7 multitasking software (version 3.2). The instrument was calibrated with indium and cyclohexane for each set of experiments.

The thermal stability of the GNCs was measured using a Perkin-Elmer TGA instrument (Pyris Diamond TG/DTA) under nitrogen atmosphere at a heating rate 10 °C/min.

g. Dynamic Mechanical Property Measurements. The storage modulus (G), loss modulus (G') and tan δ of the GNCs were measured using a dynamic mechanical analyzer (DMA) (TA Instruments model Q-800). Samples were prepared in the film form (25 mm × 5 mm × 0.15 mm) by pouring the formic acid solution on a die and evaporating it in a pool of air to dryness at 60 °C and finally in a vacuum at 60 °C for 7 days. The films were then installed in the tension clamp of a calibrated instrument. The sample was heated from 0 to 120 °C at the heating rate of 5 °C/min. The G, G', and tan δ were measured at a constant frequency of 1 Hz with a static force of 0.02 N.

h. dc Conductivity Measurement. For electrical conductivity measurements, the gels were pressed to make pellets (diameter = 1.3 cm) in a press. The conductivity was measured at room temperature (27 °C) by the standard spring-loaded pressure contact four-probe method.[44] All the samples were contacted with silver

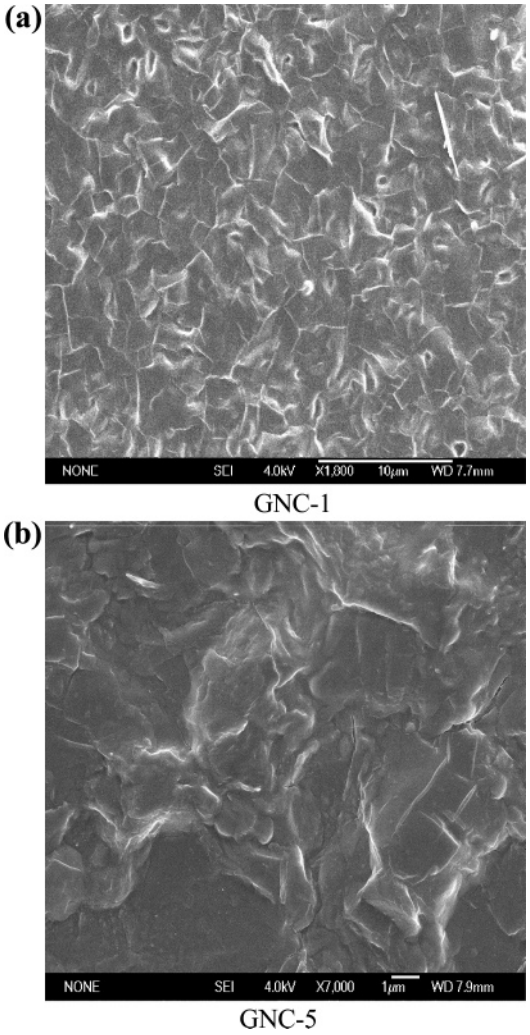

Figure 1. SEM pictures of solvent cast (a) GNC-1 and (b) GNC-5, respectively.

paste. A constant current (I) from a constant direct current source electrometer (Keithley, model 617) was allowed to pass through two diagonal leads of the four probes and the voltage (V) across the other two leads was measured using a multimeter (Keithley, model 2000). The conductivity (σ) was measured from the relation[44]

$$\sigma = (\ln 2/\pi d)\,(I/V) \qquad (1)$$

where d is the thickness of the pellet and was taken as the average of four different measurements using a screw gauge.

Results and Discussion

In parts a and b of Figure 1, the SEM pictures of GNC-1 and GNC-5 are shown, and they exhibit fibrillar network morphology. This is also true for the pure PANI−DNNDSA (15% PANI w/w) system and the GNC-3 sample (Figure 2 a and b, Supporting Information), characterizing that they also have fibrillar network structure. Thus, both PANI−DNNDSA and GNCs have fibrillar network morphology.[34,35] In Figure 2, the heating and cooling thermograms of GNC-1 are shown. In the heating curve of the as-prepared sample (thermogram (a)), two endothermic peaks at 67 and 81 °C are observed, and in the cooling curve, two exothermic peaks at 69 and 26 °C are observed. The sample on further heating also exhibit two endothermic peaks at 57 and 76 °C, indicating the reversible first-order phase transition in the system. This reversible behavior is observed in all the other systems (Figure 3, Supporting Information) irrespective of the nature of clay dispersions (intercalated or exfoliated) in the samples (see later). Thus, the fibrillar network structure and reversible first-order phase transition characterize the systems as thermoreversible gels[45] like in the pure PANI−DNNDSA systems.[34−37] The presence of nanoclay in the gels results in gel nanocomposites (GNCs), which are characterized in the following sections.

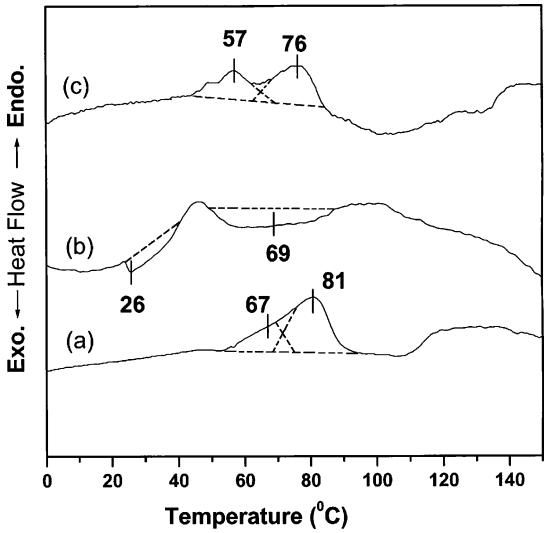

Figure 2. DSC thermograms of GNC-1 (a) first heating of the as-prepared gel from −20 °C (heating rate10 °C/min), (b) cooling from 160 °C at the cooling rate 5 °C/min up to −20 °C, and (c) second heating of the gel prepared at −20 °C for 15 min at the scan rate 10 °C/min.

Here, it is necessary to discuss the origin of double exothermic or double endothermic peaks in the DSC thermograms. This may be clarified from the model of the PANI−DNNDSA system shown in Figure 3, which has been obtained from the energy minimization using the MMX program.[46] Here, the PANI chains are anchored with DNNDSA molecules to produce a lamella structure (see below),[34−36] and the structure is then energetically minimized. Overlapping of the surfactant tails produces bilayers, and monolayers are produced where no overlapping occurs. Both monolayers and bilayers are capable of crystallization,[34−36] and the two exotherms and endotherms in Figure 2 are for monolayer and bilayer crystallization and melting, respectively. The higher melting point may be assigned for the melting of a densely packed bilayer crystal of nonyl tails and the lower melting point may be for the monolayer crystals of naphthyl heads.[34−36] The different nature of dispersion (intercalated or exfoliated) of clay tactoids in the nanocomposite would not affect the monolayer and bilayer structure of anchored DNNDSA unless the PANI−DNNDSA lamella structure is perturbed in the composites. Thus, the DSC patterns would remain the same for all composites if PANI lamella structure persists. The monolayer and bilayer crystals of anchored DNNDSA produce a lamellar structure, which supramolecularly organizes into a fibrillar structure. This fibrillar network structure is responsible for thermoreversible gel formation. The monolayer and bilayer surfactant crystals are reversibly fusible and act as junction points in the gel.

WAXS Pattern and TEM Observation. In Figure 4, the WAXS pattern of clay, om-clay, PANI−DNNDSA, and the GNCs are shown. It is clear from the figure that the lamella peak of om-clay shifted to a lower angle than that of the unmodified clay. Here, the gallery spacing shifts from 1.33 to 2.20 nm, indicating the incorporation of cetyl chains of CTAB into the gallery, replacing Na^+ and Ca^{2+}. From the diffractogram of PANI gel, it is apparent that there are two peaks at lower

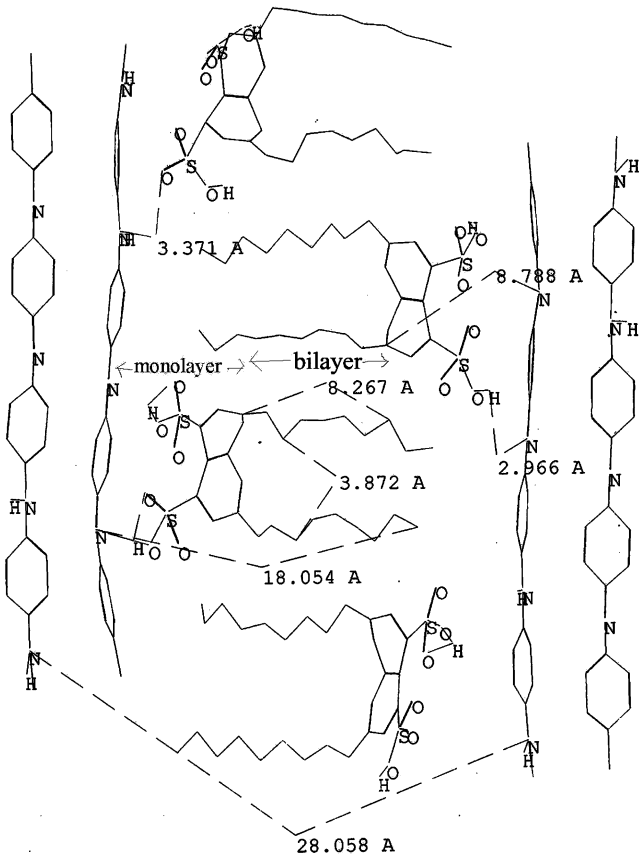

Figure 3. An approximate molecular model (energy minimized structure) of the PANI−DNNDSA system using the MMX program.

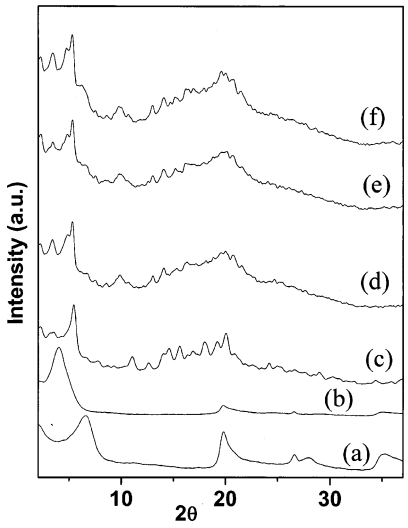

Figure 4. WAXS patterns of (a) Na−MMT clay, (b) om-clay, (c) PANI−DNNDSA, (d) GNC-1, (e) GNC-3, and (f) GNC-5.

angles ($2\theta = 3.5°$ and 5.46°), corresponding to the lamellar thickness (25.2 Å) and the thickness of a pendent DNNDSA chain (16.2 Å). This is evident from the model (Figure 3) of the PANI−DNNDSA system, where the respective distances are 28.0 and 18.0 Å. Thus, it may be concluded that the PANI−DNNDSA system has a lamellar structure with a lamellar thickness of 25.2 Å. In the gel nanocomposites (GNCs), the two diffraction peaks of the PANI−DNNDSA system is retained and the peak of om-clay is lost for all of the composites. This indicates that the om-clay lamella structure is either lost or its gallery spacing became extended such that it is beyond the instrument limit to observe the peaks. The former may produce an exfoliated structure and the latter may cause an intercalated structure. However, mixed intercalation between the PANI−DNNDSA chain and om-clay tactoids are also possible. In Table 1, the *d* spacings and the intensity ratio (I/I_0) of the various peaks of X-ray patterns are presented. The *d* spacings are of completely new origin, and the new peaks at smaller angles may arise from the crystallization of pendent DNNDSA tails anchored from the PANI chains.[34−36] Apart from the spacing of these new crystallites, the monolayer and bilayer thickness of surfactant tails and also of total thickness of the surfactant chain may be obtained from the data. A comparison of these results with that of the model indicates that the X-ray data fit approximately well with those obtained from the model. An interesting point that should be noted is that the PANI−DNNDSA distance peak at ($d = 16.2$ Å) shows an additional hump for the GNCS and it corresponds to a value of 18.7 Å. The reason for such behavior is not known to us and might arise for the mixed lamella formation between clay tactoids and the PANI−DNNDSA chain.

Table 1. d_{hkl} (Å) and Intensity Ratio (I/I_0) Values of the PANI−DNNDSA System and the GNCs

PANI−DNNDSA		GNC-1		GNC-3		GNC-5	
d_{hkl}	I/I_0	d_{hkl}	I/I_0	d_{hkl}	I/I_0	d_{hkl}	I/I_0
				39.1	87	39.6	84
		18.7	hump	18.7	hump	18.7	hump
25.2	71	26.2	82	25.9	80	26.2	86
16.2	100	16.6	100	16.6	100	16.6	100
		10.3	43				
		8.96	50	8.99	53	9.09	48
7.9	47						
7.0	41	6.79	50	6.81	52	6.82	49
		6.29	57	6.31	57	6.29	54
6.08	55						
5.68	58					5.48	60
5.26	52						
4.92	61	4.89	63			4.95	61
4.62	62					4.53	73
4.42	70	4.44	72	4.41	72		
		4.27	68				
		3.60	46				

In Figure 5, the TEM pictures of GNC-1, GNC-3, and GNC-5 are shown. From the figure, it is apparent that GNC-1 has different morphology from that of GNC-3 and GNC-5. In GNC-1, the clay tactoids are dispersed in different dispositions, indicating an exfoliated clay structure. Multiple clay platelets also coexist with the individual silicate layers in the micrograph.[7,17] Apart from the dark contrast of clay tactoids, the lighter contrast PANI−DNNDSA lamellas are also observed at different angular dispositions to the clay lamella in the micrograph (Figure 5a). An average value of PANI−DNNDSA lamellar thickness was measured from the TEM micrograph and has a value of 26 Å, which is very close to the X-ray value (25 Å) of PANI−DNNDSA lamella.

In GNC-3 and GNC-5, the morphology is quite different and intercalated clay structure is observed, i.e., the PANI− DNNDSA remains intercalated within the clay tactoids (Figure 5b and c). A careful look at the micrograph indicates that the PANI−DNNDSA lamella remains parallel to the clay tactoids in GNC-3 and GNC-5 system. But this is not true in GNC-1, where the PANI−DNNDSA lamellas are at different angular dispositions to the clay lamella. From the TEM pictures of GNC-3 and GNC-5, the dimensions of PANI−DNNDSA lamellas (lighter contrast) intercalated between the darker contrast clay tactoids was measured. It has an average value of 17.5 Å. This indicates that, during the preparation procedure, the PANI−DNNDSA

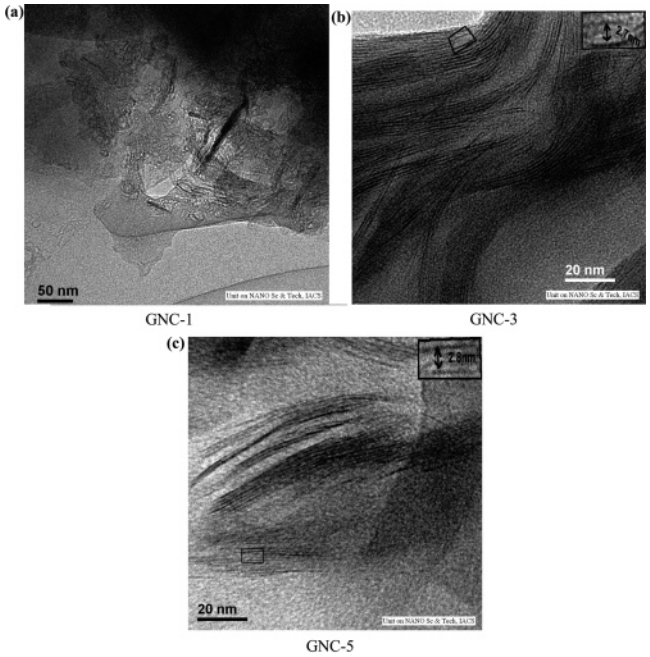

Figure 5. TEM micrographs of (a) GNC-1, (b) GNC-3, (c) GNC-5.

lamella is broken into single comblike chains and it intercalates into the om-clay lamella. Such a situation is really interesting, as a mixed lamella of om-clay tactoids and PANI−DNNDSA chains may be produced. The monolayer and bilayer crystallization might also be possible in this mixed lamella as in the PANI−DNNDSA lamella. Also, there are some lamella of thickness ~27 Å, indicating the presence of unperturbed PANI−DNNDSA lamella within the clay tactoids.

The WAXS patterns of GNC-1, GNC-3, and GNC-5 are very similar. This is because in all of the three nanocomposite structures are very similar. In all of the cases, the PANI−DNNDSA lamella is present and it shows a different peak for d_{hkl} = 26 Å (in Figure 3, it is 28 Å). The peak of d_{hkl} = 16.6 Å is due to the distance of the DNNDSA chain anchored from the PANI chain (in Figure 3, it is 18 Å). Another hump of interest is for the d_{hkl} value of 18.7 Å, which we propose for the formation of mixed lamellas of the PANI−DNNDSA chain and cetylammonium group anchored from the clay tactoids. This peak should be present in all of the three samples because, in the intercalated structures, the PANI−DNNDSA chain becomes sandwiched between om-clay tactoids, and in the exfoliated state, the mixed lamella is produced in one side of the PANI−DNNDSA chain, and in the other side, the PANI−DNNDSA lamella is produced. The smaller d_{hkl} values are almost same, indicating the crystallites produced by monolayer and bilayer crystallization are very similar in all three samples.

It is now interesting to discuss why GNC-1 produces an exfoliated structure but GNC-3 and GNC-5 produce an intercalated structure. No definite reason is known, and it may be probable that the entropy change in GNC-1 due to exfoliation of clay tactoids overcomes the small positive enthalpy value arising from the dispersion interaction between overlapping cetyl chains in the om-clay gallery. But when the clay concentration is large (GNC-2 and GNC-3), the total enthalpy change for the dispersive interaction of the clay gallery is high because of the increase of interacting sites. This high positive enthalpy value is not overcome by the entropy factor to make the free energy change negative. Consequently, intercalated structures are produced at higher clay concentration and exfoliated structures are produced at lower (e.g., 1%) clay concentration.

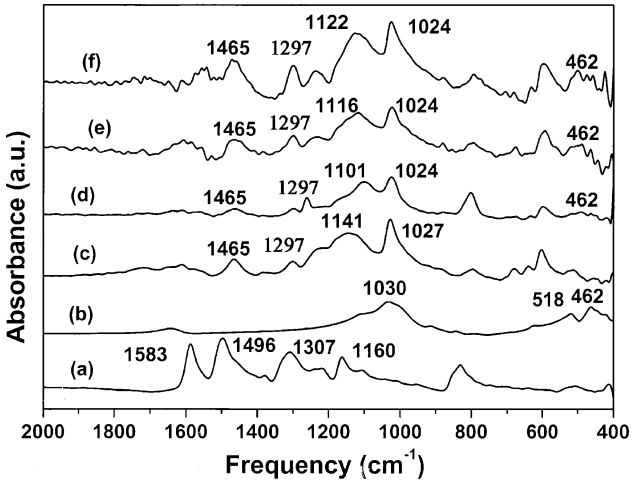

Figure 6. FTIR spectra of (a) PANI (EB), (b) om-clay, (c) PANI−DNNDSA, (d) GNC-1, (e) GNC-3, and (f) GNC-5.

Scheme 1. (a) PANI (EB) (B = benzonoid unit and Q = quinonoid unit), 1 (b) Doped PANI (polaron form), and 1 (c) Dinonylnaphthalene Disulfonic Acid (DNNDSA)

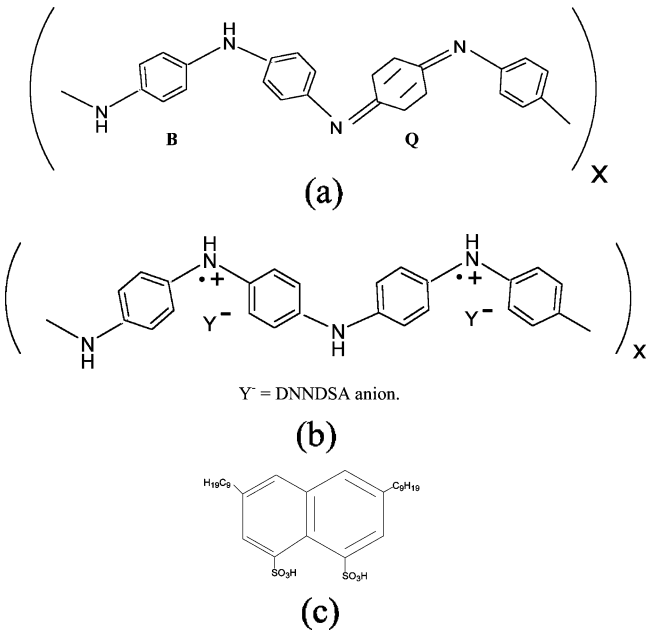

FTIR Spectra. In Figure 6, the FTIR spectra of om-clay, PANI, PANI−DNNDSA gel, and the GNCs are presented. Om-clay has characteristic peaks at 1030, 518, and 462 cm^{-1} for Si−O−Si stretching, Si−O stretching, and Si−O bending, respectively.[47] In the GNCs, the 1030 cm^{-1} peak becomes overlapped with the 1027 cm^{-1} peak of the PANI−DNNDSA gel. The other peaks are observed in the GNCs, and they gradually develop in size with increasing clay concentration. PANI has a characteristic peak at 1160 cm^{-1}, corresponding to a vibration mode of quinonoid structure (N═Q═N) of PANI (EB) with partial electronic-like character[48−51] (Scheme 1). In Scheme 1, the chemical structure of PANI (EB) and PANI (ES, emeraldine salt) forms are shown. On doping with protonic acids, the radical cations (polarons) are generated on the PANI (ES) chain, making it conducting. On addition of DNNDSA, this peak shifts to 1141 cm^{-1}, indicating that the double-bond character is lost (Q═N^+H−B or B−N^+H−B) due to polaron formation on doping (Scheme 1).[48−51] In the GNC-1, this peak further shifts to a lower energy band at 1101 cm^{-1}. A probable cause for this shift is due to the attraction of the cetyl group of om-clay to the nonyl groups of DNNDSA by dispersion

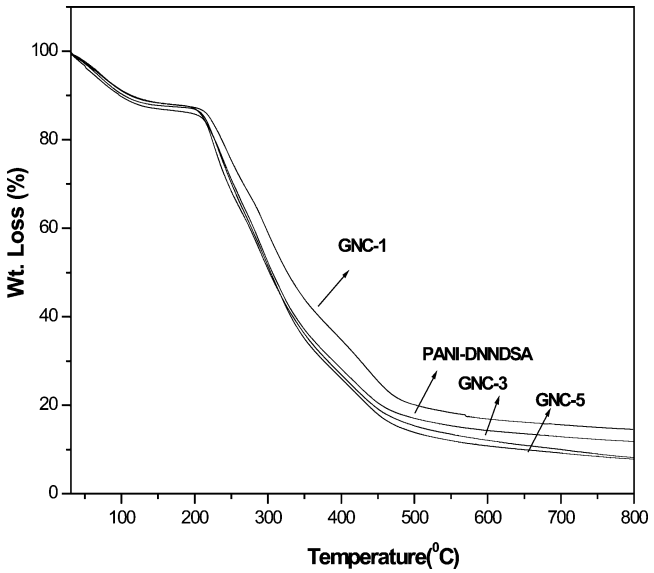

Figure 7. TGA thermograms of PANI−DNNDSA, GNC-1, GNC-3, and GNC-5 under N_2 atmosphere at 10 °C/min heating rate.

interaction. This attraction separates the DNNDSA anion from the polaron center to some extent, making the Q═N^+H−B or B−N^+H−B vibration at lower energy. The situation becomes slightly different when the PANI−DNNDSA chains become confined within the clay tactoids (GNC-3 and GNC-5). Here, the separation of the DNNDSA anion from the polaron center is less than that in the exfoliated structure (GNC-1) due to confinement of PANI−DNNDSA chains into clay tactoids. This causes an increase in the frequency of the Q═N^+H−B or B−N^+H−B vibration band (1116 and 1122 cm^{-1} for GNC-3 and GNC-5, respectively). The C−H in-plane bending vibration that also occurs in the region 1010−1170 cm^{-1} [50] has lower intensity and cannot be detected distinctly in the samples due to the broadness of the above bands in that region. The 1496 cm^{-1} of PANI (EB) is for the deformation of a benzonoid ring and it shifts to 1465 cm^{-1} in PANI−DNNDSA gel due to the protonation.[50,52] However, this band is not affected in the GNCs. Similarly, the 1307 cm^{-1} peak of PANI (EB) (C−N stretching of secondary amine) shifts to1297 cm^{-1} on addition of DNNDSA,[49] but it does not change within the GNCs. The 1583 cm^{-1} peak of PANI (EB) for quinonoid ring deformation[50,53] is lost in the PANI−DNNDSA gel. The reason is unknown, and probably it may account for the loss of quinonoid structure due to doping by the bulkier DNNDSA group.

Thermogravimetric Analysis. In Figure 7, the TGA curves of PANI−DNNDSA gel and the GNCs are shown. From the figure, it is apparent that the pure gel starts degradation at 203 °C, but the GNCs degrade at 213, 203, and 206 °C for 1%, 3%, and 5% clay concentration, respectively. The residual weight is also higher for GNC-1 than that of pure gel, and for GNC-3 and GNC-5, it is lower than that of pure gel. This certainly indicates GNC-1 is stabler than all other GNCs and pure gel probably due to the exfoliated nature of the clay tactoids on the gel matrix. Here, the exfoliated clay particles act as barriers to heat flow due to their high aspect ratio and thereby hinder the degradation process. But this is not true for the intercalated structures, where they exhibit easier degradation that is unusual in polymer clay nanocomposites.[17,54] However, there are also reports where a decrease in degradation temperature occurs with increase in clay concentration.[7,18] The reason of easier degradation of GNC-3 and GNC-5 compared with PANI−DNNDSA gel is not known. It might be possible for the mixed lamella formation between the PANI−DNNDSA chain and cetylammonium group anchored clay tactoids, making an easier heat transfer to the PANI chains.

Mechanical Properties. Usually, in polymer−clay nanocomposites, the mechanical properties of the nanocomposite are dramatically enhanced. The storage modulus, loss modulus, and tan δ plots of GNCs are presented in Figure 8a−c. From Figure 8a, it is apparent that storage modulus of each system decreases with increase in temperature from 0 to 120 °C. Below 0 °C, the measurement was difficult due to cracking of the sample films at lower temperature. It is interesting to note that the storage modulus of GNCs has increased more dramatically than that of pure gel and the increase is highest for GNC-1. For GNC-3 and GNC-5, GNC-3 has a higher storage modulus value than that of GNC-5. In Table 2, the storage modulus values and its increase from that of PANI−DNNDSA gel are presented. From the table, it is apparent that there is 233% increase of storage modulus for GNC-1 at 0 °C, and at 60 °C, the increase is 445%. For GNC-3 and GNC-5, the reinforcement effect is lower than that of GNC-1. The reinforcement effect is caused for the large surface area and high aspect ratio of the clay tactoids. The probable explanation for the highest reinforcement of GNC-1 is that the clay tactoids are in an exfoliated state, which yields randomly dispersed clay tactoids, but this is not true for the interlamellar structure where the clay tactoids are very closely spaced. The surface area of exfoliated clay tactoids is fully available for reinforcement, but in the intercalated structures, the surface area of the clay tactoids is not totally available due to closer packing, and as a result, weaker reinforcement occurs in the intercalated structure. The decrease in storage modulus value for GNC-5 than for GNC-3 might be due to some agglomeration of clay tactoids at the higher concentration. In Figure 5c, thicker clay tactoids are seen, but it is not observed in Figure 5b. It should be noted here that, with increase in temperature, the reinforcement effect (Table 2) increases, indicating that the system becomes more viscoelastic with increasing temperature. However, after gel melting temperature (∼76 °C), the storage modulus increase is lower. This is probably due to the melting of network junctions (monolayer and bilayer crystals) that make the system elastic, and at the gel melting temperature, the network transforms into a sol, losing the elastic property.

It is now necessary to compare the storage modulus value reported in the literature for the PANI−clay system.[7,55] Yeh et al. reported the storage modulus value of PANI equal to 1500

Table 2. Storage Modulus of PANI−DNNDSA and the GNCs

	PANI−DNNDSA	GNC-1		GNC-3		GNC-5	
temperature (°C)	storage modulus (MPa)	storage modulus (MPa)	% increase	storage modulus (MPa)	% increase	storage modulus (MPa)	% increase
0	549	1277	233	1091	199	809	147
30	190	625	329	512	269	387	204
60	66	294	445	210	318	145	220
85	21	42	200	36	171	40	190

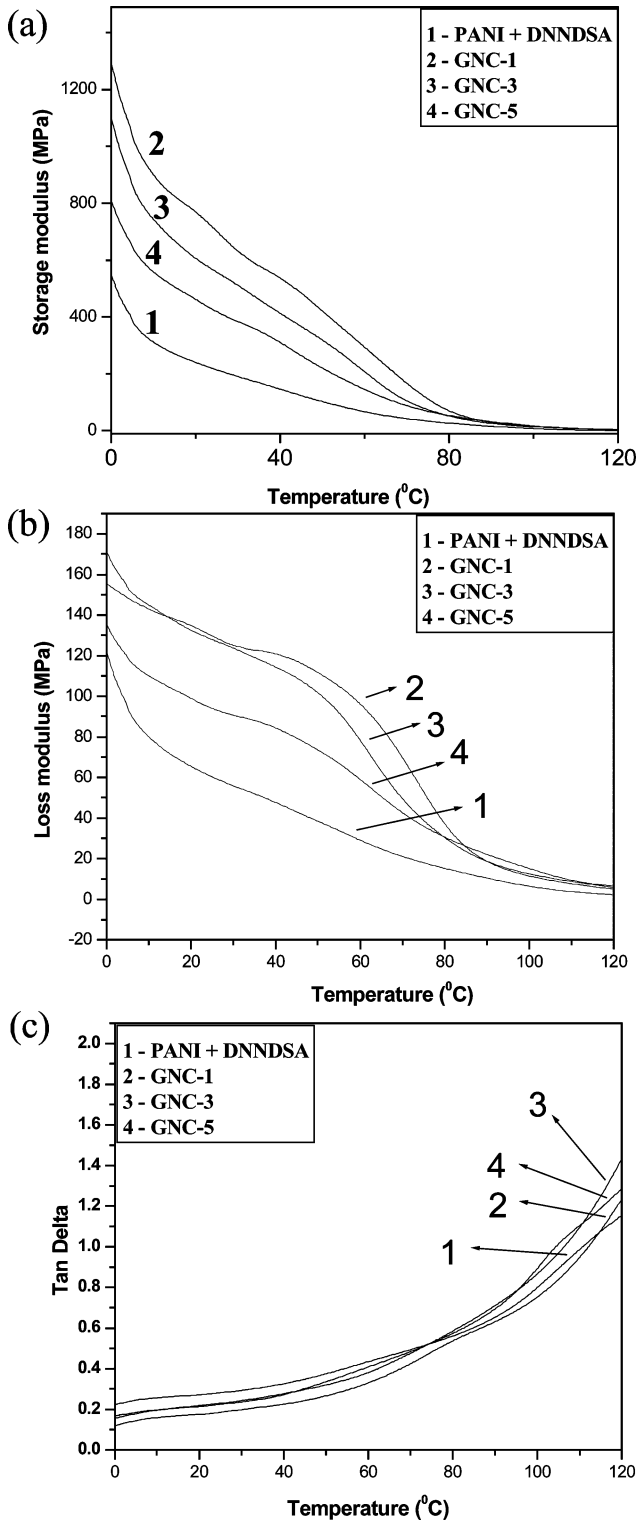

Figure 8. Mechanical property variation of PANI−DNNDSA, GNC-1, GNC-3, and GNC-5 with temperature: (a) storage modulus, (b) loss modulus, and (c) tan δ.

MPa at 30 °C.[7] In our case, the PANI−DNNDSA gel has the storage modulus value of 190 MPa. This may be quite relevant, as in the gel, there is 85% (w/w) DNNDSA, which has a negligible storage modulus value at room temperature due to its gummy nature. On addition of clay during in situ polymerization, Yeh et al. observed a decrease in modulus value of PANI with the addition of clay, eg., 0.5% and 0.75% clay yielded the storage modulus values 1200 and 730 MPa, respectively.[7] However, in their case, the molecular weight of PANI had

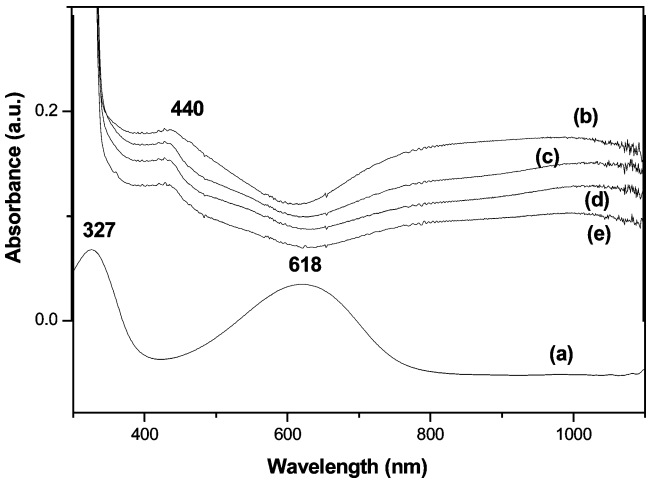

Figure 9. UV−Vis spectra of (a) PANI (EB), (b) PANI−DNNDSA (c) GNC-1, (d) GNC-3, and (e) GNC-5 in DMF at 30 °C.

decreased during the polymerization with clay, so the effect of clay on the storage modulus cannot be directly compared. In this regard, we want to discuss the poly(3-hexyl thiophene)−clay nanocomposite data, as the system when prepared from the solvent-cast method has network structure but when prepared from the melt cooled state has no network structure.[17,18] The percent increase of storage modulus on addition of clay is greater for the sample prepared in the solvent-cast method than that in the melt-cooled method. As for example, for the sample of P3HT with 1% clay, the increase of G' is 600% at 20° C, but for the sample prepared from the later method, the increase is only 41%. This large increase of storage modulus in the solvent-cast method may be attributed for the network structure in the solvent-cast P3HT film. Here also, such a large increase (445%) in storage modulus of GNC-1 might be due to the network structure of PANI gel. This is because the network structure makes the system more viscoelastic where the reinforcement effect of clay is very high.

In Figure 8b, the loss modulus vs temperature plots are shown. Storage modulus relates the ability of a material to store or return energy, whereas the loss modulus relates the ability to lose the energy when oscillatory force is applied to the specimen. Here, the loss modulus shows a decrease with temperature for each system like the storage modulus plot (Figure 8a), and its variation with clay concentration remains almost the same as that of the storage modulus. Therefore, it may be argued that the increase of loss modulus with clay concentration is due to the same reason as the storage modulus increase as discussed above. In Figure 8c, tan δ is plotted with the temperature for the GNCs, and it gradually increases with temperature for all the cases. The monotonic variation in all these cases indicates that there is no α or β relaxation for this system within the temperature range studied here.

UV−Vis Spectra. In Figure 9, the UV−vis spectra of PANI (EB), PANI−DNNDSA, and the GNCs in DMF are presented. It is apparent from the figure that PANI (EB) has peaks at 327 nm corresponding to the $\pi-\pi^*$ transition of the benzonoid ring and a 618 nm peak for electronic excitation from benzonoid ring to quinonoid ring.[56−58] In the PANI−DNNDSA gel and in the GNCs, the 618 nm peak is absent and a new peak at ~856 nm appears, indicating doping is complete in all the PANI−DNNDSA systems. Another new peak at 440 nm also appears in these doped systems corresponding to the polaron band to π^* band transition. The 856 nm peak corresponds to the π band to localized polaron band transition,[57,58] and the absence of any

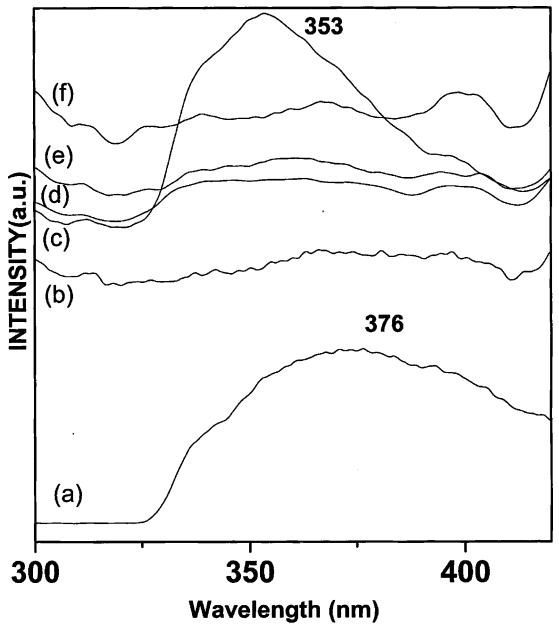

Figure 10. Photoluminescence spectra of (a) DNNDSA, (b) PANI (EB), (c) PANI−DNNDSA, (d) GNC-5, (e) GNC-3, and (f) GNC-1 after excitation by radiation of 226 nm wavelength at 30 °C.

free carrier tail indicates absence of a delocalized polaron. In the GNCs, clay has no influence on the UV−vis spectra, indicating the band gap of the π band to polaron band transition is not affected in the nanocomposites.

Photoluminescence Spectra. In Figure 10, the fluorescence spectra of PANI−DNNDSA and that of the GNCs are presented. It is apparent from the figure that PANI (EB) has no emission after excitation at 226 nm, but the DNNDSA shows an emission peak at 376 nm. In the pure PANI−DNNDSA gel, the emission occurs at 353 nm. This new peak may arise from the benzonoid structure of doped PANI, but a benzonoid group adjacent to a quinonoid structure (as in PANI (EB)) does not yield any luminescence.[59,60] Some contribution of photoluminescence from the unreacted DNNDSA may also be present in the PANI−DNNDSA gel. Thus, the present PANI−DNNDSA gel has a photoluminescence property. On the addition of clay, quenching in the photoluminescence emission occurs in all the GNCs. In GNC-1, the clay has an exfoliated structure, and as a result, both intra- and interchain energy transfer and energy transfer through the clay tactoids is permissible, causing a nonradiative luminescence spectra. But in GNC-3 and GNC-5, the PANI−surfactant chains remains intercalated, and as a result, the interchain energy transfer will be less.[17,18] So in this case, the quenching would be somewhat less than that of GNC-1, and the spectra d and e of Figure 10 corroborate the same.

Conductivity. The dc conductivity of GNCs are 0.76×10^{-2}, 0.617×10^{-2}, 1.32×10^{-2}, and 0.627×10^{-2} S/cm for PANI−DNNDSA, GNC-1, GNC-3, and GNC-5, respectively. Pure PANI−DNNDSA gel has a conductivity of 10^{-2} order as reported earlier.[34,35] On the addition of clay, the conductivity of the GNCs remain almost same. The probable explanation may be obtained from the UV−vis spectra (Figure 9), where the π band to polaron band transition peak is in the same position (856 nm). Consequently, the band gap is the same for both the pure gel and also in the GNCs. This results in the same conductivity of the gel and the GNCS. This is really an interesting observation, where the mechanical property is enhanced by 445% by the nanoclay without altering the conductivity.

Conclusion

The PANI−DNNDSA system has the characteristics of thermoreversible gel when prepared from formic acid medium. The gel structure remains intact on the addition of om-clay, producing a gel nanocomposite. The GNCs exhibit reversible first-order phase transition. TEM and WAXS data indicate that the GNC-1 has an exfoliated structure, whereas GNC-3 and GNC-5 have an intercalated structure. The GNC-1 exhibits the highest thermal stability due to the exfoliated nature of the clay tactoids. FTIR spectra indicate that the Q═N^+H−B or B−N^+H−B vibration of PANI−DNNDSA occurs at a lower frequency due to the interaction with om-clay. The effect is more prominent in the exfoliated clay structure than that in the intercalated clay structure. The storage modulus has increased dramatically (445%) by the addition of om-clay, and the increase is the highest for the exfoliated clay structure. With increase in temperature, the percent increase of the storage modulus increases for each system, but after the gel melting temperature, it decreases. The π band to polaron band transition peak remains unaffected in the GNCs and so also the conductivity. Though PANI (EB) does not show any emission, the PANI−DNNDSA gel exhibits photoluminescence. In the GNCs, photoluminescence quenching occur more in the exfoliated state than in the intercalated state. These GNCs of PANI are easily processable due to its thermoreversible nature.

Acknowledgment. We gratefully acknowledge the Council of Scientific and Industrial Research (grant No-01-(1919)/04/EMR-II), New Delhi, for financial support. Also, the financial support from the Department of Science and Technology under the Nanoscience and Nanotechnology Program is gratefully acknowledged. The help extended by King Industries, Norwalk, CT, for the gift sample of DNNDSA is also gratefully acknowledged.

Supporting Information Available: FTIR spectra of dried PANI-DNNDSA gel and GNCs, indicating absence of formic acid and isobutanol. Scanning electron micrograph of dried samples of PANI−DNNDSA and GNC-3. DSC thermograms of GNC-3 and GNC-5. This material is available free of charge via the Internet at http://pubs.acs.org.

References and Notes

(1) Vaia, R. A.; Krishnamoorti, R. In *Polymer Nanocomposites: Synthesis Characterization and Modeling*; Krishnamoorti, R., Vaia, R. A., Eds.; American Chemical Society: Washington, D C, **2001**, p 1.
(2) Giannelis, E. P.; Krishnamoorti, R.; Manias, E. *Adv. Polym. Sci.* **1999**, *138*, 107.
(3) Okamoto, M.; Morita, S.; Kim, Y. H.; Kotaka, T.; Tateyama, H. *Polymer* **2001**, *42*, 1201.
(4) Fornes, T. D.; Yoon, P. J.; Keskkula, H.; Paul, D. R. *Polymer* **2001**, *42*, 9929.
(5) Alexandre, M.; Dubois, P. *Mater. Sci. Eng. Rev.* **2000**, *R28*, 1.
(6) Park, J. H.; Jana, S. C. *Macromolecules* **2003**, *36*, 2758.
(7) Yeh, J.-M.; Liou, S.-J.; Lai, C.-Y.; Wu, P.-C.; Tsai, T.-Y. *Chem. Mater.* **2001**, *13*, 1131.
(8) Lee, T.-W.; Park, O O.; Kim, J.-J.; Hong, J.-M.; Kim, Y. C. *Chem. Mater*. **2001**, *13*, 2217.
(9) do Nascimento, G. M.; Constantino, V. R. L.; Temperini, M. L. A. *Macromolecules* **2002**, *35*, 7535.
(10) Goddard, Y. A.; Vold, R. L.; Hoatson, G. L. *Macromolecules* **2003**, *36*, 1162.
(11) Kim, B.-H.; Jung J.-H.; Hong, S.-H.; Joo, J.; Epstein, A. J.; Mizoguchi, K.; Kim, J. W.; Choi, H. J. *Macromolecules* **2002**, *35*, 1419.
(12) do Nascimento, G. M.; Constantino, V. R. L.; Landers, R.; Temperini, M. L. A. *Macromolecules* **2004**, *37*, 9373.
(13) Kim, B. H.; Jung, J. H.; Kim, J. W.; Choi, H. J.; Joo, J. *Synth. Met.* **2001**, *117*, 115.
(14) Jia, W.; Segal, E.; Kornemandel, D.; Lamhot, Y.; Narkis, M.; Siegmann, A. *Synth. Met.* **2002**, *128*, 115.

(15) Bae, W. J.; Kim, K. H.; Jo, W. H.; Park, Y. H. *Macromolecules* **2004**, *37*, 9850.
(16) Liu, Y.-C.; Tsai, C.-J. *Chem. Mater.* **2003**, *15*, 320.
(17) Kuila, B. K.; Nandi, A. K. *Macromolecules* **2004**, *37*, 8577.
(18) Kuila, B. K.; Nandi, A. K. *J. Phys. Chem. B* **2006**, *110*, 1621.
(19) Yeh, J.-M.; Chen, C. L.; Chen, Y.-C.; Ma, C.-Y.; Lee, K. R.; Wei, Y.; Li, S. X. *Polymer* **2002**, *43*, 2729.
(20) Yeh, J.-M.; Chin, C. P.; *J. Appl. Polym. Sci.* **2003**, *88*, 1072.
(21) Yeh, J.-M.; Chin, C.-P.; Chang, S. *J. Appl. Polym. Sci.* **2003**, *88*, 3264.
(22) Kingsborough, R. P.; Swager, T. M. *Adv. Mater.* **1998**, *10*, 1100.
(23) Focke, W. W.; Wnek, G. E.; Wei, Y. *J. Phys. Chem.* **1987**, *91*, 5813.
(24) Cao, Y.; Andreatta, A.; Heeger, A. J.; Smith, P. *Polymer* **1989**, *30*, 2305.
(25) Gettinger, C. L.; Heeger, A. J.; Pine, D. J.; Cao, Y. *Synth. Met.* **1995**, *74*, 81.
(26) Vikki, T.; Pietila, L.-O.; Osterholm, H.; Ahjopalo, L.; Takala, A.; Toivo, A.; Levon, K.; Passiniemi, P.; Ikkala, O. *Macromolecules* **1996**, *29*, 2945.
(27) Kinlen, P. J.; Liu, J.; Ding, Y.; Graham, C. R.; Remsen, E. E. *Macromolecules* **1998**, *31*, 1735.
(28) Kababya, S.; Appel, M.; Haba, Y.; Titelman, G. I.; Schmidt, A. *Macromolecules* **1999**, *32*, 5357.
(29) Paul, R.K.; Pillai, C. K. S. *Synth. Met*. **2000**, *114*, 27.
(30) Menon, R.; Yoon, C. O.; Moses, D.; Heeger, A. J. In *Handbook of Conducting Polymers*, 2nd ed.; Skotheim, T. A., Elsenhaumer, R. L., Reynolds, J. R., Eds.; Marcel Dekker Inc.; New York, 1998, p 27.
(31) Olinga, T. E.; Fraysse, J.; Travers, J. P.; Dufresne, A.; Pron, A. *Macromolecules* **2000**, *33*, 2107.
(32) Vikki, T.; Ruokolainen, J.; Ikkala, O. T.; Passiniemi, P.; Isotalo, H.; Torkkeli, M.; Serimaa, R. *Macromolecules*, **1997**, *30*, 4064.
(33) Vikki, T.; Isotalo, H.; Ruokolainen, J.; Passiniemi, P.; Ikkala, O. *Synth. Met.* **1999**, *101*, 742.
(34) Jana, T.; Nandi, A. K. *Langmuir* **2000**, *16*, 3141.
(35) Jana, T.; Nandi, A. K. *Langmuir* **2001**, *17*, 5768.
(36) Jana, T.; Chatterjee, J.; Nandi, A. K. *Langmuir* **2002**, *18*, 5720.
(37) Jana, T.; Roy, S.; Nandi, A. K. *Synth. Met.* **2003**, *132*, 257.
(38) Yano, K.; Usuki, A.; Okada, A.; *J. Polym. Sci., Polym. Chem. Ed.* **1997**, *35*, 2289.
(39) Zhu, J.; Morgan, A. B.; Lamelas, F. J. Wilkie, C. A. *Chem. Mater*. **2001**, *13*, 3774.
(40) Andreatta, A.; Cao, Y.; Chiang, J. C.; Heeger, A. J.; Smith, P. *Synth. Met.* **1988**, *26*, 383.
(41) Baird, D. G.; Smith, J. K. *J. Polym. Sci, Polym. Chem. Ed.* **1978**, *16*, 61.
(42) Usuki, A.; Kawasumi, M.; Kojima, Y.; Okada, A.; Kurauchi, T.; Kamigaito, O. *J. Mater. Res.* **1993**, *8*, 1174.
(43) Clothup, N. B.; Daly, L. H.; Wiberley, S. E. *Introduction to Infrared and Raman Spectroscopy*; Academic Press: New York, 1964.
(44) Frommer, J. E.; Chance, R. R. In *Encyclopedia of Polymer Science Engineering*, 2nd ed.; Mark, H. F., Bikales, N. M., Overberger, C. G., Menges, G., Eds.; John Wiley & Sons, Inc.: New York, 1986; Vol. 5, p 473.
(45) Daniel, C.; Dammer, C.; Guenet, J. M. *Polymer* **1994**, *35*, 4243.
(46) Gajewski, K. I.; Gilberr, M. H. In *Advances in Molecular Modeling*; Liotta, D., Ed.; JAI Press: Greenerick, CT, 1990; Vol. 2.
(47) Darder, M.; Colilla, M.; Ruiz-Hitzky, E. *Chem. Mater.* **2003**, *15*, 3774.
(48) (a) Palaniappan, S.; Nivasu, V. *New. J. Chem.* **2002**, *26*, 1490. (b) Tang, J.; Jing, X.; Wang, B.; Wang, F. *Synth. Met.* **1988**, *24*, 231. (c) Salaneck, W. R.; Liedberg, B.; Inganas, O.; Erlandsson, R.; Lundstrom, I.; MacDiarmid, A. G.; Halpern, M.; Somasiri, N. L. D. *Mol. Cryst. Liq. Cryst*. **1985**, *121*, 191. (d) Zengin, H.; Zhou, W.; Jin, J.; Czerw, R.; Smith, D. W., Jr.; Echegoyen, L.; Carroll, D. L.; Foulger, S. H.; Ballato, J. *Adv. Mater.* **2002**, *14*, 1480.
(49) Hatchett, D. W.; Josowicz, M.; Janata, J. *J. Phys. Chem. B.* **1999**, *103*, 10992.
(50) Stejskal, J.; Trchova, M.; Prokes, J.; Sapurina, I. *Chem. Mater*. **2001**, *13*, 4083.
(51) Qiu, H.; Wan, M.; Matthews, B.; Dai, L. *Macromolecules* **2001**, *34*, 675.
(52) Stejskal, J.; Sapurina, I.; Trchova, M.; Prokes, J.; Krivka, I.; Tobolkova, E. *Macromolecules* **1998**, *31*, 2218.
(53) Furukawa, Y.; Ueda, F.; Hyodo, Y.; Harada, I.; Nakajima, T.; Kawagoe, T. *Macromolecules* **1988**, *21*, 1297.
(54) Yeh, J.-M.; Liou, S.-J.; Lin, C.-Y.; Cheng, C.-Y.; Chang, Y.-W.; Lee, K.-R. *Chem. Mater.* **2002**, *14*, 154.
(55) Kim, J. W.; Kim, S. G.; Choi, H. J.; Jhon, M. S. *Macromol. Rapid Commun.* **1999**, *20*, 450.
(56) (a) Stejskal, J.; Kratochvil, P.; Radhakrishnan, N. *Synth. Met.* **1993**, *61*, 225. (b) Huang, W. S.; MacDiarmid, A. G. *Polymer* **1993**, *34*, 1833.
(57) Xia, Y.; Wiesinger, J. M.; MacDiarmid, A. G.; Epstein, A. J. *Chem. Mater.* **1995**, *7*, 443.
(58) Ruokolainen, J.; Eerikainen, H.; Torkkeli, M.; Serimaa, R.; Jussila, M.; Ikkala, O. *Macromolecules* **2000**, *33*, 9272.
(59) Thorne, J. R. G.; Masters, J. G.; Williams, S. A.; MacDiarmid, A. G.; Hochstrasser, R. M. *Synth. Met.* **1992**, *49/50*, 159.
(60) Shimano, J. Y.; MacDiarmid, A. G. *Synth. Met.* **2001**, *123*, 251.

MA060636W